Journal of
Applied
Crystallography
ISSN 0021-8898

Received 11 May 2013
Accepted 9 September 2013

Effect of Mg doping on the growth aspects, crystalline perfection, and optical and thermal properties of congruent $LiNbO_3$ single crystals

B. Riscob,[a,b,c] Indranil Bhaumik,[d] S. Ganesamoorthy,[e] R. Bhatt,[d] N. Vijayan,[a] A. K. Karnal,[d] M. A. Wahab[b] and G. Bhagavannarayana[a]*

[a]CSIR–National Physical Laboratory, Dr K. S. Krishnan Road, New Delhi 110 012, India, [b]Department of Physics, Crystal Growth and XRD Laboratory, Jamia Millia Islamia, New Delhi 110 025, India, [c]Institute for Plasma Research, Bhat, Gandhinagar, Gujarat 382 428, India, [d]Laser Materials Development and Devices Division, Raja Ramanna Centre for Advanced Technology, Indore, Madhya Pradesh 452 013, India, and [e]X-ray Scattering and Crystal Growth Section, Condensed Matter Physics Division, Material Science Group, IGCAR, Kalpakkam, Tamil Nadu 603 102, India. Correspondence e-mail: bhagavan@nplindia.org

Mg-doped congruent lithium niobate single crystals were grown by the Czochralski technique. High-quality single crystals were grown using a novel seeding technique in a resistive heating furnace. Analysis of crystalline perfection carried out by a multi-crystal X-ray diffractometer revealed that the grown crystals do not contain any structural grain boundaries but do contain point defects. The transmission characteristics showed an enhancement of band gap with an increase in Mg concentration. Conoscopy patterns revealed that the grown crystals are homogeneous and the incorporation of Mg into the lattice does not affect the optical sign (negative uniaxial) of the crystal. The refractive index measurements carried out using a prism coupler showed an increase in the optical birefringence (Δn), while the refractive index was found to decrease with the increase in doping concentration. Further, thermal conductivity was found to decrease with Mg incorporation in the lattice owing to phonon scattering from the Mg ions and, as a consequence, at high concentrations (>4 mol%) crack formation occurred. However, optimization of growth conditions reveals that a slower pulling rate leads to crack-free lithium niobate crystals even at 6 mol% Mg doping.

1. Introduction

Although the successful growth of lithium niobate (LN) was reported quite a long time ago (Ballman, 1965), it is still being explored for new applications with different dopants (Kokanyan *et al.*, 2004; Kong *et al.*, 2007). Pure LN is used in areas of research such as electro-optic modulators, second harmonic generators, Q-switches, surface acoustic wave filters *etc*. Bulk crystals of doped $LiNbO_3$ are important for a variety of applications, especially those related to nonlinear optical (Byer, 1997), ferroelectric (Nassau *et al.*, 1966) and photo-refractive effects (Buse, 1997). Single crystals of LN can be grown as the congruent composition (cLN) (Riscob *et al.*, 2013), *i.e.* with an Li/Nb molar ratio of 48.6:51.4, as well as the stoichiometric composition (sLN), *i.e.* 50:50. Although sLN has several advantages as it has fewer defects, the growth of good optical quality single crystals is tedious. At the same time a number of major breakthroughs have taken place in the growth of cLN in terms of the improvement in controlling defects to suit the applications (Lerner *et al.*, 1966). However, device performance in the case of electro-optic and high-power laser applications is limited in both sLN and cLN because of laser-induced refractive index inhomogeneities (Ashkin *et al.*, 1966). In LN single crystals, a variety of dopants has been investigated by different researchers to increase optical damage resistance (Zhen *et al.*, 2003; Schlarb & Betzler, 1994; Yamamoto *et al.*, 1992; Volk *et al.*, 1994). Normally, in the case of pure LN, device performance is greatly affected as a result of a change in the refractive index in high-power laser experiments for nonlinear applications. In the 1980s it was reported that doped LN samples have 100 times the optical stability to withstand a high-power optical source (laser) in comparison with pure LN (4.6 mol% MgO was added to the host material; Zhong *et al.*, 1980). Mg doping removes the antisite Nb (Nb_{Li}^{4+}) defects and improves the optical damage resistance significantly by increasing the photoconductivity and thus reducing the magnitude of the light-induced refractive index changes. In recent times MgO–LN has attracted attention because of its high optical damage resistance. There are various reports available about its crystal growth (Grabmaier & Otto, 1986; Furukawa *et al.*, 1990; Hu, Chang, Yen *et al.*, 1991), phase equilibrium (Grabmaier & Otto, 1986; Zhou *et al.*, 1991), defect structure (Zhang & Feng,

1991; Sweeney *et al.*, 1985), characterization and properties (Shen *et al.*, 1992; Zhou *et al.*, 1990).

Generally, a congruent composition of LN leads to inherent point defects during growth, which generate geometric strain and lattice distortion in the crystalline matrix. However, when it is doped with dopants like Mg to mask its defects, specifically an Li vacancy (with a view to improving its efficiency), the system can respond in a different manner, leading to changes in the point defect distribution, the formation of dislocations (Bhagavannarayana *et al.*, 2010) and finally the appearance of structural boundaries (Bhagavannarayana, Ananthamurthy *et al.*, 2005). These defects sometimes mask or cause a partial/complete deterioration in some of the anisotropic physical properties of single crystals and reduce the efficiency of devices made out of these crystals (Tsai *et al.*, 2008; Bhagavannarayana *et al.*, 2006). Therefore, to realize the full efficiency of the devices, the crystal must be free from such structural defects (Bhagavannarayana, Budakoti *et al.*, 2005) and hence its crystalline perfection should be assessed before its active usage, particularly when it is doped. It is equally important to understand the perfection of the crystal at different doping levels, as the crystalline perfection strongly depends on the amount and size of the introduced dopant(s) in the crystal lattice (Bhagavannarayana *et al.*, 20006; Bhagavannarayana & Kushwaha, 2010), and thereby, if necessary, one may find a way to optimize the crystal growth conditions to grow a good-quality crystal at a required doping level. A variety of instrumentation techniques such as X-ray topography, Fourier transform infrared (FTIR), Raman spectroscopy, electron paramagnetic resonance, nuclear magnetic resonance and transmission electron microscopy have been employed to characterize LN crystals for structural defects (Yan *et al.*, 2004; Wallace, 1970; Sidorov *et al.*, 2007; Sugh *et al.*, 1973; Ivanova *et al.*, 1980; Wicks & Lewis, 1968). However, high-resolution X-ray diffractometry (HRXRD) is found to be one of the most efficient, convenient and nondestructive tools to assess the structural perfection of single crystals, particularly to assess point defects and the low- and very low angle structural grain boundaries (Bhagavannarayana *et al.*, 2006; Kumar *et al.*, 2011). In this article, we report the growth of high-quality LN single crystals and the effect of Mg doping on the crystalline perfection by using HRXRD. Further, the influence of Mg on the optical band gap, conoscopy, refractive index and thermal properties of cLN is also investigated.

2. Experimental

2.1. Crystal growth

High-quality single crystals of Mg-doped LN were grown with different Mg concentrations of 2, 4 and 6 mol%. A Cyberstar-make automatic diameter controlling crystal puller coupled with an $MoSi_2$-based furnace was used for the current growth experiment. The resistive heating furnace helps to maintain a low thermal gradient in the growth zone, which reduces the probability of cracking and produces a good-quality single crystal. The thermal gradient in the furnace was adjusted by varying the position of the crucible during trial experiments. The thermal gradient increases on lifting the crucible from the central zone towards the top of the furnace, but in that case a large temperature oscillation appears, leading to the formation of growth striations in the crystal as a result of thermal instability at the growth interface. Platinum crucibles were used for the present experiment for the growth of crystals and R-type thermocouples were used to measure the temperature of the molten charge. The heating and cooling were controlled using a Eurotherm 902 (single loop) proportional-integral-derivative (PID)-based programmable temperature controller with a resolution of 0.01 K. The high-purity raw materials of Li_2CO_3 (99.999%) and Nb_2O_5 (99.99%) were used in the proportions 48.46 and 51.54 mol%, respectively, to obtain the congruent composition. The material was synthesized by solid-state reaction after proper ball milling. A good quality z-cut seed was used for the present experiment, and the rotation and pulling rate were controlled precisely by a Cyberstar crystal puller to be 25 r min^{-1} and 3 mm h^{-1}, respectively.

2.2. High-resolution X-ray diffraction

The crystalline perfection of the grown single crystals was investigated by HRXRD by employing a multi-crystal X-ray diffractometer developed at the National Physical Laboratory, New Delhi (Lal & Bhagavannarayana, 1989). A well collimated and monochromated Mo $K\alpha_1$ beam obtained from three monochromator Si crystals set in dispersive (+,−,−) configuration was used as the exploring X-ray beam. The specimen crystal is aligned in the (+,−,−,+) configuration. Because of the dispersive configuration, though the lattice constant of the monochromator crystal(s) and the specimen are different, the unwanted dispersion broadening in the diffraction curve (DC) of the specimen crystal is insignificant. The specimen can be rotated about the vertical axis, which is perpendicular to the plane of diffraction, with a minimum angular interval of 0.4″. The rocking or diffraction curves were recorded by changing the glancing angle (the angle between the incident X-ray beam and the surface of the specimen) around the Bragg diffraction peak position θ_B (taken as zero for the sake of convenience), starting from a suitable arbitrary glancing angle and ending at a glancing angle after the peak so that all the meaningful scattered intensities on both sides of the peak are included in the DC. The DC was recorded by the so-called ω scan, wherein the detector was kept at the same angular position $2\theta_B$ with a wide opening for its slit. This arrangement is very appropriate for recording the short-range-order scattering caused by defects or by scattering from local Bragg diffraction from agglomerated point defects or due to low-angle and very low angle structural grain boundaries (Bhagavannarayana & Kushwaha, 2010; Kumar *et al.*, 2011). Before recording the DC, in order to remove the surface damage incurred during cutting and polishing of the sample, the samples are ground, lapped and then etched with a non-preferential etch of HNO_3 and HF in a 2:1 ratio at a room temperature of 303 K for 10 min.

2.3. UV–Vis–NIR spectroscopy

The optical transparency and absorption spectra were measured in the UV–Vis–NIR region of the specimen using a commercial Jasco V-263 spectrophotometer. The measurements were carried out with unpolarized light at normal incidence at room temperature.

2.4. Conoscopic studies

The conoscopic study was carried out using an Olympus polarized optical microscope.

2.5. Prism coupler spectroscopy

For the present measurement a commercial Prism coupler (model 2010/M; manufactured by Metricon Corporation, UK) was used. The refractive index was measured using the methodology described by Bhaumik *et al.* (2011).

2.6. Thermal studies

Specific heat (C_p) measurement was carried out using a Mettler Toledo Star simultaneous differential scanning calorimetry (DSC) analyser at a heating rate of 10 K min^{-1} in a nitrogen atmosphere using an alumina crucible. The heat flow of the sample DSC was measured with respect to temperature and time in a controlled atmosphere using sapphire as a reference to measure C_p.

The thermal diffusivity measurement was carried out using an LFA 1000-Linseis by the laser flash measurement method.

3. Results and discussion

3.1. Crystal growth

Single crystals were grown by the Czochralski (Cz) method under a low thermal gradient using a resistive heated furnace. Top seeding was employed for the growth with a z-cut seed. Bhaumik *et al.* (2002) reported an interesting aspect of seeding in potassium titanyl phosphate growth, which yielded good-quality crystals in an optimum condition. We have adopted a similar kind of seeding technique in the present experiment, as shown in Fig. 1. Here, during seeding the solid–liquid interface was maintained at a level above the molten charge using the surface tension force of the melt. The grain boundaries that are normally formed from the seed portion during growth were reported by Bhagavannarayana *et al.* (2011). The importance of the present growth method is that it allows us to avoid such grain boundaries within the seed portion while growing a few inches of seed with controllable size before coming to the necking portion, which precedes the cylindrical portion.

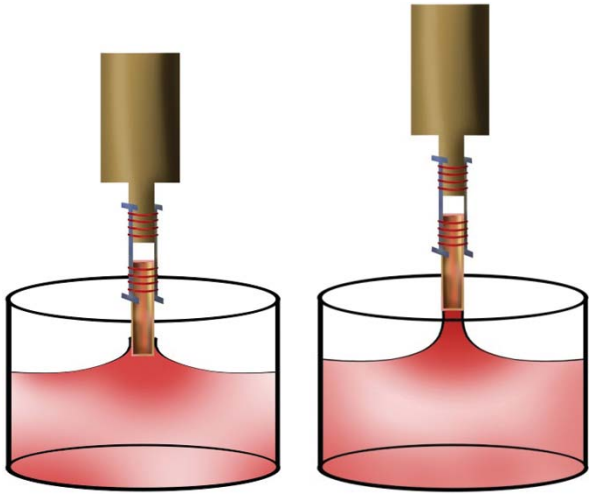

Figure 1
Drawing of the seeding technique used for the present LN growth.

Initially all the crystals with different doping concentrations were grown with the same pulling and rotation rates of 3 mm h^{-1} and 25 r min^{-1}, respectively. Although we obtained a crack-free crystal for 2 and 4 mol% of doping concentration (Figs. 2*a* and 2*b*), in the case of the 6 mol%-doped crystal, cracks were formed which could be seen with the naked eye (Fig. 2*c*). The cracking may be due to the low thermal conductivity in the crystal with a high doping concentration, and this is discussed in detail in §3.6. However, a good-quality crack-free crystal of 6 mol%-doped crystal could be grown with a pulling rate of 1 mm h^{-1}, as shown in Fig. 2(*d*).

3.2. High-resolution X-ray diffractometry

Fig. 3 shows the high-resolution DCs recorded for a set of three LN crystals using the (006) diffracting planes in sym-

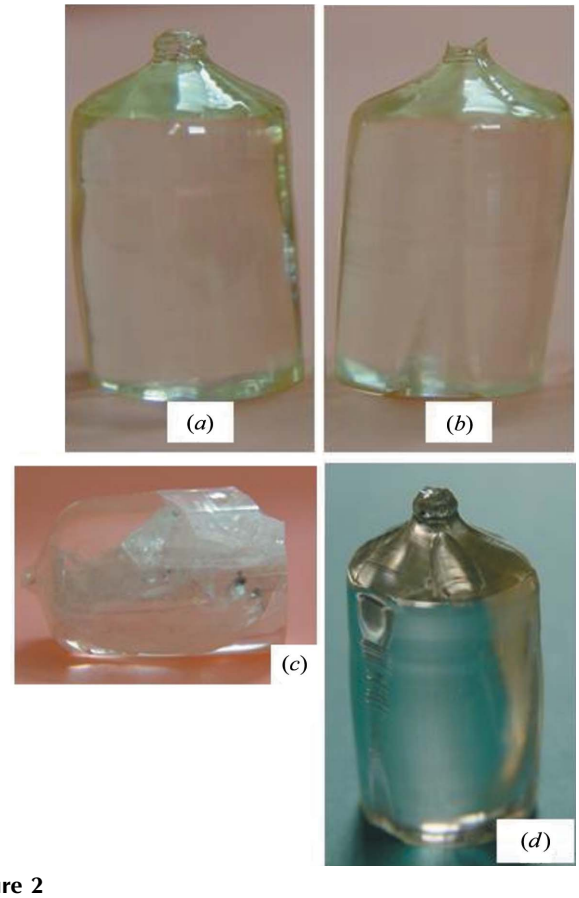

Figure 2
Photograph of Cz-grown Mg:cLN single crystals: (*a*) 2 mol%, (*b*) 4 mol%, (*c*) 6 mol% cracked crystal and (*d*) 6 mol% uncracked crystal.

metrical Bragg geometry with Mo $K\alpha_1$ radiation. The curves (*a*), (*b*) and (*c*) are, respectively, for a pristine crystal, a 2 mol% Mg-doped LN crystal and a 4 mol% Mg-doped LN crystal. All these curves are drawn with the same scale for both the ordinate and abscissa to readily determine the relative intensity of peaks and FWHM (full width at half-maximum) values. These crystals were grown under identical growth conditions with a pulling rate of 3 mm h^{-1} and post-growth cooling of 100 K h^{-1}. As seen in the figure, the DCs of all the specimens contain a single diffraction peak without any satellite peak(s), showing that these crystals do not contain any internal structural grain boundaries, which are otherwise very commonly observed in LN crystals (Bhagavannarayana, Ananthamurthy *et al.*, 2005). Though all the DCs have single curves, there are some interesting and distinguishing features in these curves. The FWHM of curve (*a*) is 29″. Though this value is somewhat higher than that expected from the plane-wave theory of dynamical X-ray diffraction (Batterman & Cole, 1964), *i.e.* 2.6″ (Kushwaha, Maurya *et al.*, 2011), it is quite comparable to the earlier reported values of 21″ (Bhatt *et al.*, 2011) and 62″ (Kushwaha *et al.*, 2012). This indicates the presence of a low density of point defects and their aggregates, which are unavoidable in real-life crystals because of thermodynamical effects. The FWHM of curve (*b*) is 76″, and this substantially higher value compared to that of the pure crystal indicates that Mg doping leads to a substantial increase in point defects. The FWHM value of ∼110″ of curve (*c*) belonging to the 4 mol% Mg-doped specimen shows that an increase in doping from 2 to 4 mol% causes the value of the FWHM to increase substantially, which in turn shows the enhanced density of point defects as expected because of additional doping.

It is interesting to discuss the area under these curves, which is also known as the integrated intensity (ρ) and gives rich information about the defect structure, particularly in the doped/implanted crystals (Bhagavannarayana & Kushwaha, 2010; Lal *et al.*, 1991). The value of ρ for a particular crystal and for a particular set of diffracting planes is always higher for a crystal having a mosaic or defect structure than for an almost perfect crystal without any defects, because of extinction or anomalous absorption along the direction of Bragg angles (Kushwaha, Vijayan *et al.*, 2011). The ratio of estimated values of ρ for the pure (Fig. 3*a*), 2 mol% Mg-doped (Fig. 3*b*) and 4 mol% (Fig. 3*c*) Mg-doped crystals is 1:1.84:2.18. This ratio clearly indicates that the dopants are occupied in the crystalline matrix, as a consequence of which the crystals are bound to experience some strain. However, the strain is within the elastic limit and does not introduce any structural grain

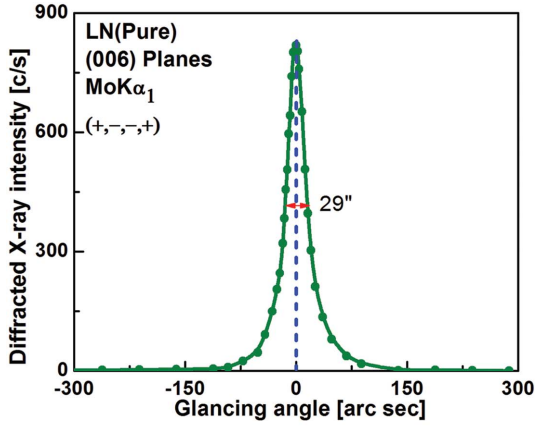

(*a*)

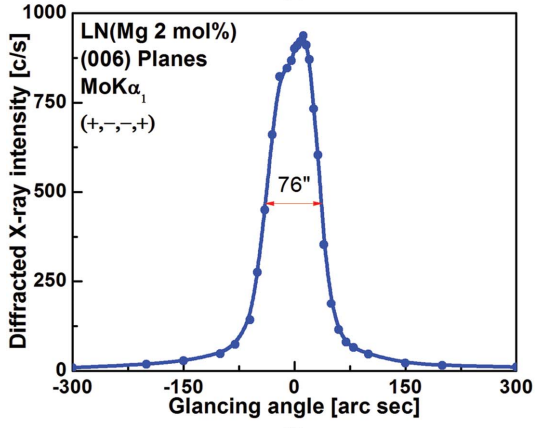

(*b*)

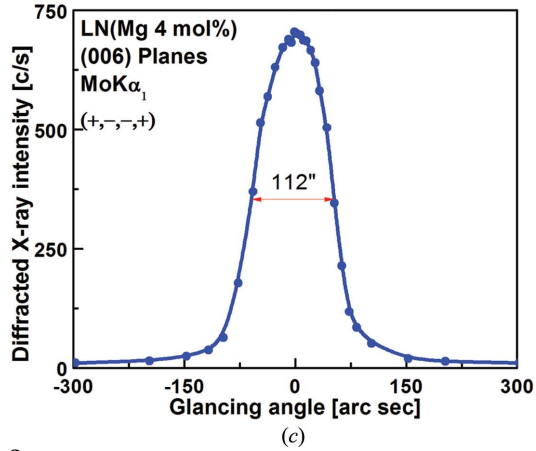

(*c*)

Figure 3
Diffraction curve recorded for LN single crystals using (006) diffracting planes with Mo $K\alpha_1$ radiation: (*a*) undoped specimen, (*b*) 2 mol% Mg-doped specimen and (*c*) 4 mol% Mg-doped specimen.

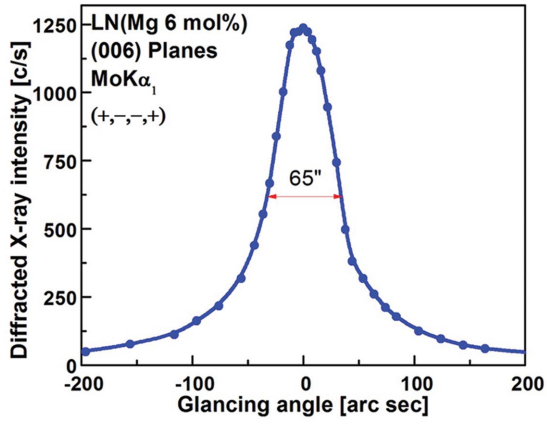

Figure 4
Diffraction curve recorded for LN single-crystal specimen grown with 6 mol% doping of Mg. The curves were recorded under the same experimental conditions as those of Fig. 3.

boundaries, which is clear from the absence of additional peaks in the rocking curves.

Crystals were also grown with 6 mol% Mg doping with the same growth conditions as maintained for the crystals discussed above. However, because of excess strain, these crystals could not be sustained and cracks formed at this high concentration. However, at a low pulling rate of 1 mm h^{-1} and cooling rate of 50 K h^{-1}, crystals at 6 mol% Mg doping were successfully grown without any cracks. Fig. 4 shows the DC for such a crystal recorded under identical conditions as those of Fig. 3. As seen in the figure, this DC also contains a single peak, showing the absence of the boundaries that are otherwise common in crystals at higher doping levels. The FWHM value is 65″, which is still lower than that of the crystals grown with 2 and 4 mol% doping level, but higher than that of the pure crystal. One interesting feature of this curve in comparison with the other curves is that the scattered intensity due to dopants at the wings is higher, as expected, because of the higher doping in this crystal. However, the lower FWHM in comparison with the DCs of Figs. 3(*b*) and 3(*c*) reveals that the dopants are well distributed within the crystalline matrix. These findings clearly indicate that the pulling rate has a great influence on the crystalline perfection and it is also clear that LN crystals can be doped at 6 mol% Mg. The value of ρ for this crystal is 2.02 times that of the undoped crystal and is slightly less than that of Fig. 3(*b*); this confirms that the crystal grown at the slower rate has better crystalline quality than the 2 mol% Mg-doped specimen, as also indicated by the value of the FWHM.

3.3. UV–Vis–NIR absorption analysis

Optical spectroscopy plays a crucial role in the characterization of nonlinear optical materials. Mg-doped LN is a useful nonlinear optical material having potential device applications. The polished single crystals of Mg-doped LN samples were cut along the growth direction with a thickness of ∼1 mm and were used for the present experimental measurements. Fig. 5(*a*) shows the transmittance spectrum which was recorded in the wavelength region 200–1200 nm; a good transmittance is observed in the visible region of the spectrum.

The variation of Mg concentration influences the absorption edges of spectra towards the blue region of the spectrum. Fig. 5(*b*) shows the calculated absorption coefficient (α) for the Mg-doped LN samples. The fundamental absorption edge is defined as the corresponding wavelength where the absorption coefficient (α) is equal to 20 cm^{-1} (λ_{20}) (Kovács *et al.*, 1997). The measured absorption edges for the Mg-doped cLN samples are 313.6 nm (2 mol%), 310.4 nm (4 mol%) and 310 nm (6 mol%) at $\alpha \simeq 20$ cm^{-1}. The observed shift in the UV absorption edge to the lower wavelength region in comparison with the reported pure cLN (Kushwaha *et al.*, 2012; Bhatt *et al.*, 2012) confirmed the reduction of lithium vacancies (V_{Li}) in the grown crystal in accordance with the Mg concentration.

The direct and indirect band-gap energies were analysed using the empirical Tauc relation (Tauc, 1972): $\alpha h\nu \propto (h\nu -$

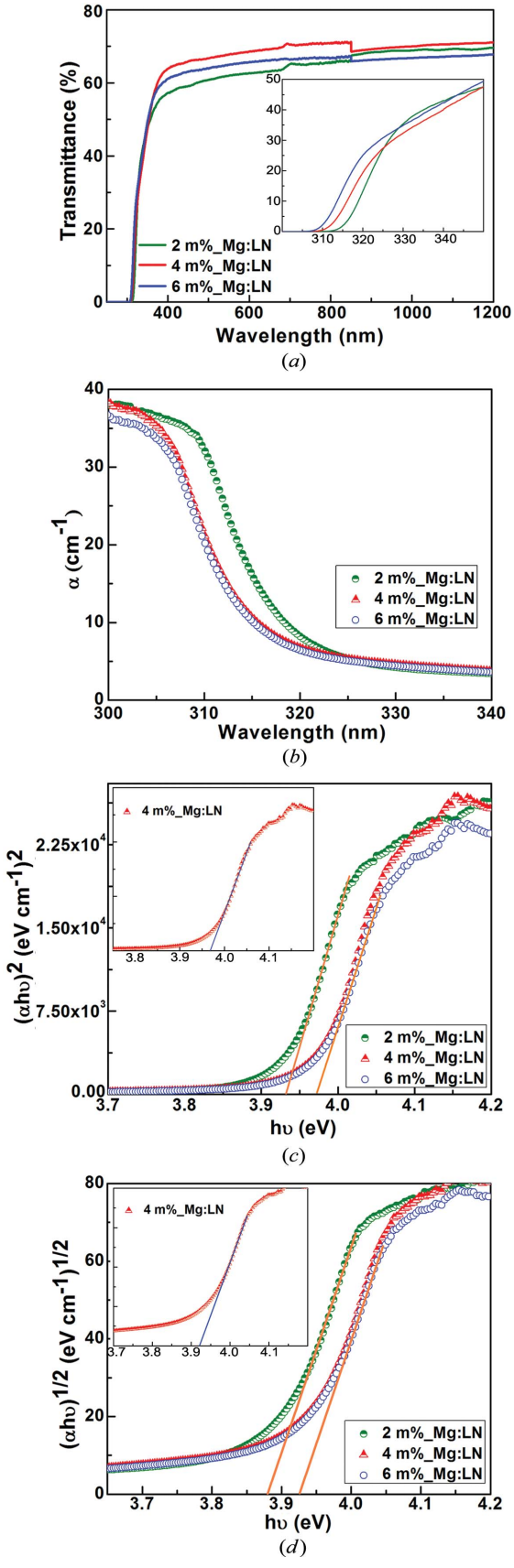

Figure 5
UV–Vis–NIR. (*a*) Transmission spectra, (*b*) absorption coefficient, (*c*) plot of direct band gap and (*d*) plot of indirect band gap of Mg:cLN single crystals.

Table 1
Direct and indirect band-gap energies of Mg-doped LN samples along with absorption edge (AE).

Sample	AE (nm)	E_g^d (eV)	E_g^{ind} (eV)	Reference
Pure cLN	318	3.93	3.74	Bhatt *et al.* (2012)
2 mol% Mg:cLN	313.6	3.93	3.87	Present work
4 mol% Mg:cLN	310.4	3.96	3.92	Present work
6 mol% Mg:cLN	310	3.97	3.93	Present work

$E_g)^m$, where $h\nu$ is the photon energy, E_g is the band-gap energy and m is an exponent determined by the nature of the electron transition during the absorption process, *i.e.* $m = 1/2$ for direct transition and $m = 2$ for indirect transition. Fig. 5(*c*) shows the plot of $(\alpha h\nu)^2$ *versus* $h\nu$ that describes the direct band-to-band transition processes and gives a detailed view of the direct band gap (E_g^d). The steep rise in absorption and the linear fit at higher photon energy shows the direct allowed interband transition (Bhatt *et al.*, 2012). The observed increase in band-gap energy for Mg-doped samples with increasing Mg concentration illustrates a decrease in structural intrinsic defects (Li vacancies and Nb_{Li}^{5+} defects); this leads to an increase in photoconductivity and hence enhanced optical damage resistance ability of the Mg-doped LN crystal system. A similar trend has also been observed in the indirect band-gap measurement. Fig. 5(*d*) shows the plot of $(\alpha h\nu)^{1/2}$ *versus* $h\nu$, where the intercept of the straight line gives the indirect band-gap energy (E_g^{ind}). The numerical values for the direct and indirect band gap are given in Table 1.

3.4. Conoscopic analysis

The shape and symmetry of the conoscopy pattern reveal information about homogeneity and strain in the crystal. The observed symmetrical fringe patterns for all the grown crystals (Fig. 6*a*–6*c*) reveal good compositional and hence optical homogeneity and the absence of residual strain in the grown crystals.

In order to examine the effect of impurities on the birefringence behaviour and particularly on the optical sign of the crystal, a retarder plate (532 nm) was introduced in the optical path and we observed the interference pattern. The birefringence behaviour does not change with doping, *i.e.* the LN crystal remains negative uniaxial after Mg doping with different concentrations, and a detailed explanation is given in the following section. The blue appearance in the second and fourth quadrants Figs. 6(*d*)–6(*f*) indicates the negative optical sign of the crystals.

3.5. Refractive index and birefringence analysis

The ordinary (no) and extraordinary (ne) refractive indices of Mg-doped cLN and pure cLN were determined at 532 and 1064 nm. Both the ordinary (no) and extraordinary refractive indices (ne) were found to decrease on Mg doping in cLN, as shown in Figs. 7(*a*) and 7(*b*). However the values of birefringence increased on Mg incorporation in the lattice (Fig. 7*c*). Also the birefringence ($\Delta n = no - ne$) value of cLN was found to be higher at 532 nm than at 1064 nm, and the same trend was observed in the case of Mg:cLN samples as well. The reduction in refractive index and enhancement of the birefringence in the presence of doping at both the wavelengths are in agreement with reported results (Schlarb & Betzler, 1994; Hu, Chang, Lin *et al.*, 1991). The observed reduction in the refractive index of the doped samples at both wavelengths may be due to modifications in the defect structure, particularly the decrease in intrinsic defects due to Mg doping. This influences the linear optical properties, which can be seen in terms of an increase in the band-gap energy as well. Further, refractive index (n) is related to the band-gap energy (E_g) by the empirical relation $n2 \simeq 1 + c/E_g$, where c is a material-dependent constant (Wempal & Didomenico, 1969). The observed decrease in the refractive index with Mg doping is in agreement with the shift of absorption edge (AE) towards higher photon energies (higher band-gap energy) (Bhatt *et al.*, 2012; Wempal & Didomenico, 1969).

3.6. Thermal conductivity

The thermal conductivity of the Mg-doped LN samples was calculated through the basic thermal parameters and as shown

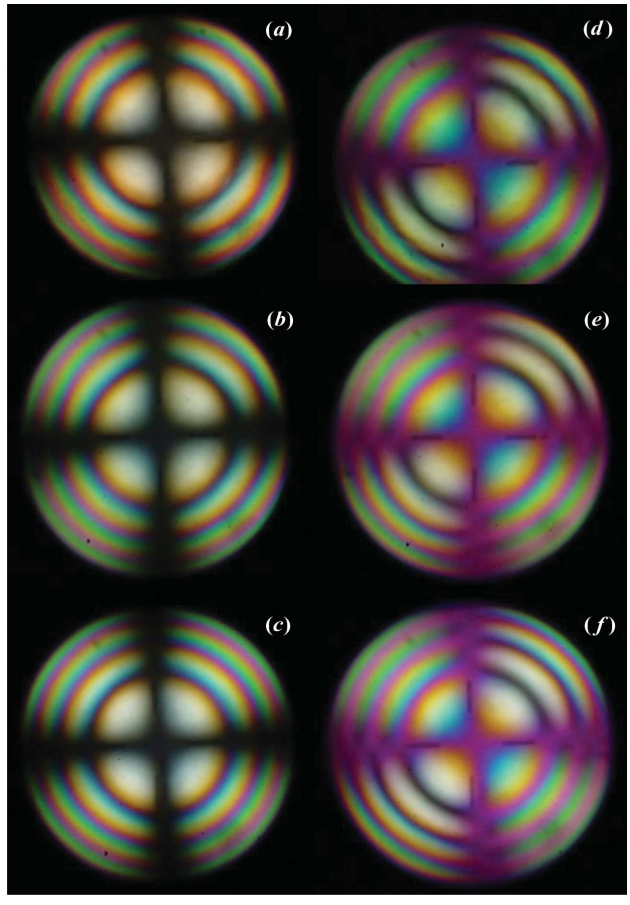

Figure 6
(*a*), (*b*) and (*c*) Conoscopy patterns for Mg:cLN crystals at 2, 4 and 6 mol% Mg doping, respectively. (*d*), (*e*) and (*f*) Insertion of a retarding λ waveplate changed the colour of the second and fourth quadrants from yellow to blue (lower wavelength side), revealing that the crystal is of a negative uniaxial type.

in Fig. 8(*a*). In the present experiment, the thermal conductivity was calculated using the relation

$$\kappa = \rho\lambda C_{\mathrm{p},} \qquad (1)$$

where κ is the thermal conductivity, ρ is the solid density of the material, λ is the thermal diffusivity coefficient and C_{p} is the specific heat capacity of the material.

Thermal diffusion coefficient measurements were carried out in the range of 298–773 K and the results are shown in Fig. 8(*b*). From these measurements, we observed that λ decreases with increasing temperature.

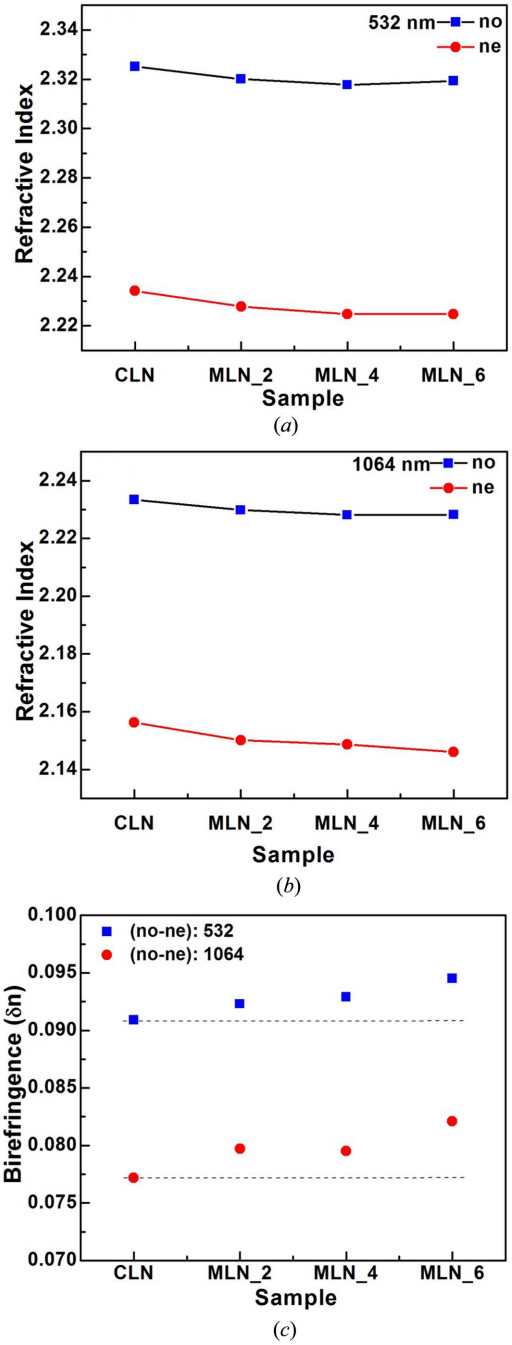

Figure 7
Refractive index of Mg:cLN single crystals at two different wavelengths: (*a*) 532 nm, (*b*) 1064 nm. (*c*) Birefringence of Mg:cLN.

The specific heat capacity (C_{p}) of Mg-doped LN samples was measured for powder samples in the temperature range of 298–773 K, as shown in Fig. 8(*c*).

The phonon transport in the material and the presence of defects play a crucial role in thermal conductivity. In general thermal conductivity decreases on adding dopants, relative to the host material, as the dopant will act as a lattice defect in the phonon transport mechanism (McMillen *et al.*, 2011). In the present experiment it was noticed that the Mg:LN crystals grown with congruent composition exhibit higher thermal conductivity in comparison to the reported value for pure cLN [3.539 W $(\mathrm{mK})^{-1}$] crystals at room temperature (Yao *et al.*, 2008). This is because Mg reduces the defect concentration in

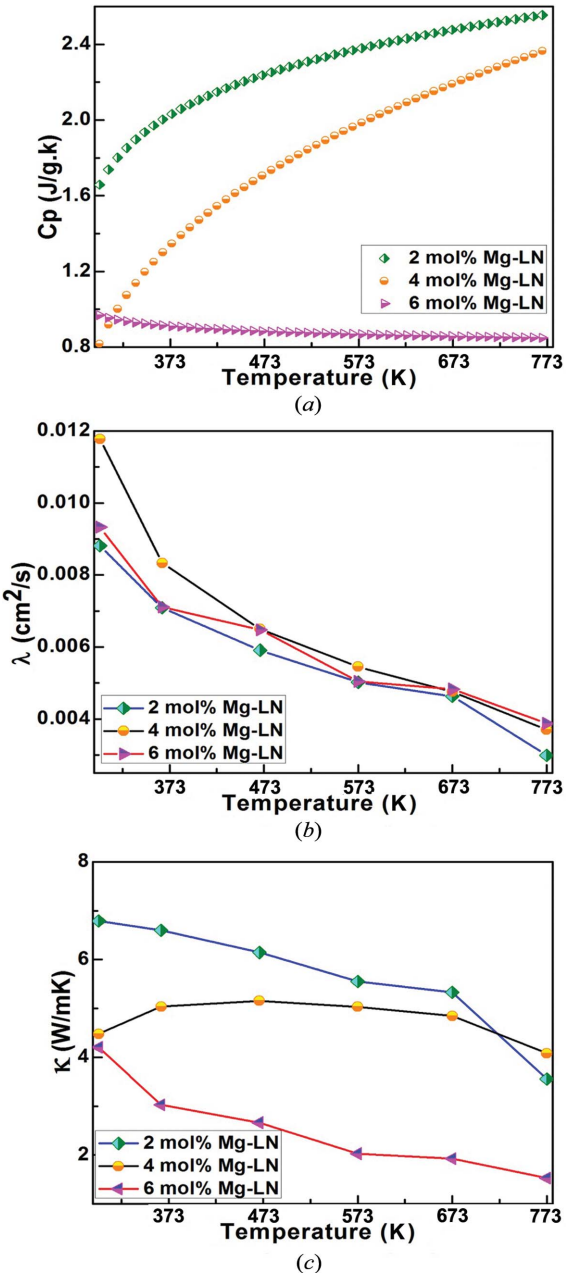

Figure 8
(*a*) Specific heat capacity, (*b*) thermal diffusivity and (*c*) thermal conductivity of Mg:cLN single crystals.

cLN, as discussed earlier, and thus reduces the overall phonon scattering processes in the sample. However, the value is comparable to that for the stoichiometric sample [5.234 W $(mK)^{-1}$] (Yao *et al.*, 2008). This is expected as sLN contains much fewer defects than cLN.

In the present measurement it was also observed that the thermal conductivity of Mg:cLN decreases upon increasing the concentration of dopant. In general, in comparison with the stoichiometric composition, the congruent composition is formed with the vacancy type of defects which can be minimized by adding Mg up to the threshold level. The scattering process of the phonons may be from the vacancies, impurities (dopant), other phonons or from grain boundaries. In the present case it is possible that, even after removing the vacancy defects, the phonon movements are controlled by higher scattering which may be due to incorporated Mg ions. Further, in general, the thermal conductivity was found to decrease with increasing temperature for all the samples as the concentration of phonons increases, resulting in more phonon–phonon scattering and leading to shortening of the mean free path of the phonon. A similar trend is observed in the thermal diffusivity plot, which is also related to the mean free path of phonons.

The lower thermal conductivity of the 6 mol% Mg-doped sample has a direct correlation with the growth aspects, as discussed in an earlier section. In the Czochralski technique the main parameters for crystal growth are diameter control and pulling rate, which are closely related to the thermal conductivity of a material (Fedulov *et al.*, 1965). Also crack formation takes place during post-growth cooling, and in order to avoid such types of cracks one should understand the thermal conductivity of the material, which limits its cooling rate (Brice, 1965). In the present experiment it was observed that the 6 mol% doped crystals are more prone to inclusion and crack formation during growth, which may be because of the low thermal conductivity in comparison with the other two samples as seen in the thermal conductivity measurements. After changing the growth parameter, specifically by decreasing the growth rate, good-quality crystals were grown.

4. Conclusions

A high-quality Mg-doped LN single crystal has been successfully grown under optimized conditions using a resistive heating furnace. The observed single peak in the HRXRD result confirmed that the grown crystal is free from grain boundaries but contains point defects. The improvement in the crystalline perfection of the 6 mol% doped sample is due to a low growth rate. The band-gap analysis shows that the Mg dopant increased the energy difference between bands. The conoscopic analysis reveals that the grown crystals are optically homogeneous and do not contain any residual strain. The refractive index, measured at 532 and 1064 nm, decreases with the increase in dopant concentration, whereas the birefringence value was found to increase with an increase in concentration. The low value of thermal conductivity (κ) observed for 6 mol% Mg-doped samples indicates that incorporation of a high Mg concentration promotes crack formation during growth of the crystal. However, even at a high doping concentration good-quality crystals have been grown by controlling the growth parameters.

The authors acknowledge Professor R. C. Budhani, Director, NPL, and Dr P. K. Gupta, Head, LMDDD, RRCAT, for their encouragement and support. The authors also acknowledge B. K. Sajith, RRCAT, for his technical support during crystal growth activity, and Dr Ajay Dhar and Dr S. K. Dawan, NPL, New Delhi, for thermal conductivity studies. BR acknowledges the Council of Scientific and Industrial Research (CSIR) for the award of Senior Research Fellowship (SRF) – 31/1/(384)/2012-EMR-I.

References

Ashkin, A., Boyd, G. D., Dziedzic, J. M., Smith, R. G., Baliman, A. A., Levinstein, J. J. & Nassau, K. (1966). *Appl. Phys. Lett.* **9**, 72–74.
Ballman, A. A. (1965). *J. Am. Ceram. Soc.* **48**, 112–113.
Batterman, B. & Cole, H. (1964). *Rev. Mod. Phys.* **36**, 681–717.
Bhagavannarayana, G., Ananthamurthy, R. V., Budakoti, G. C., Kumar, B. & Bartwal, K. S. (2005). *J. Appl. Cryst.* **38**, 768–771.
Bhagavannarayana, G., Budakoti, G., Maurya, K. & Kumar, B. (2005). *J. Cryst. Growth*, **282**, 394–401.
Bhagavannarayana, G. & Kushwaha, S. K. (2010). *J. Appl. Cryst.* **43**, 154–162.
Bhagavannarayana, G., Kushwaha, S. K., Shakir, Mohd. & Maurya, K. K. (2011). *J. Appl. Cryst.* **44**, 122–128.
Bhagavannarayana, G., Parthiban, S. & Meenakshisundaram, S. (2006). *J. Appl. Cryst.* **39**, 784–790.
Bhagavannarayana, G., Rajesh, P. & Ramasamy, P. (2010). *J. Appl. Cryst.* **43**, 1372–1376.
Bhatt, R., Ganesamoorthy, S., Bhaumik, I., Karnal, A. K., Bhagavannarayana, G. & Gupta, P. K. (2011). *J. Optoelectron. Adv. Mater.* **13**, 245–250.
Bhatt, R., Ganesamoorthy, S., Bhaumik, I., Karnal, A. & Gupta, P. (2012). *J. Phys. Chem. Solids*, **73**, 257–261.
Bhaumik, I., Bhatt, R., Ganesamoorthy, S., Saxena, A., Karnal, A. K., Gupta, P. K., Sinha, A. K. & Deb, S. K. (2011). *Appl. Opt.* **50**, 6006–6010.
Bhaumik, I., Ganesamoorthy, S., Bhatt, R., Sundar, R., Karnal, A. & Wadhawan, V. (2002). *J. Cryst. Growth*, **243**, 522–525.
Brice, J. C. (1965). *J. Cryst. Growth*, **42**, 42730–42737.
Buse, K. (1997). *Appl. Phys. B Lasers Opt.* **64**, 391–407.
Byer, R. L. (1997). *J. Nonlinear Opt. Phys. Mater.* **6**, 549–592.
Fedulov, S. A., Shapiro, Z. I. & Ladyzhinskii, P. B. (1965). *Sov. Phys. Crystallogr.* **10**, 218–220.
Furukawa, Y., Sato, M., Nitanda, F. & Ito, K. (1990). *J. Cryst. Growth*, **99**, 832–836.
Grabmaier, B. & Otto, F. (1986). *J. Cryst. Growth*, **79**, 682–688.
Hu, L., Chang, Y., Lin, I. & Yang, S. (1991). *J. Cryst. Growth*, **114**, 191–197.
Hu, L. J., Chang, Y. H., Yen, F. S., Lin, S. P., Lin, I. & Lin, W. Y. (1991). *J. Appl. Phys.* **69**, 7635–7639.
Ivanova, Z. I., Kovrigin, A. I., Luchinskĭi, G. V., Rashkovich, L. N., Rubinina, N. M. & Kholodnykh, A. I. (1980). *Sov. J. Quantum Electron.* **10**, 577–580.
Kokanyan, E. P., Razzari, L., Cristiani, I., Degiorgio, V. & Gruber, J. B. (2004). *Appl. Phys. Lett.* **84**, 1880–1882.
Kong, Y., Liu, S., Zhao, Y., Liu, H., Chen, S. & Xu, J. (2007). *Appl. Phys. Lett.* **91**, 081908.
Kovács, L., Ruschhaupt, G., Polgar, K., Corradi, G. & Wohlecke, M. (1997). *Appl. Phys. Lett.* **70**, 2801–2803.

Kushwaha, S. K., Maurya, K. K., Vijayan, N. & Bhagavannarayana, G. (2011). *CrystEngComm*, **13**, 4866–4872.
Kushwaha, S. K., Maurya, K. K., Vijayan, N., Kumar, B., Bhatt, R., Ganesamoorthy, S. & Bhagavannarayana, G. (2012). *CrystEngComm*, **14**, 3297–3305.
Kushwaha, S. K., Vijayan, N., Maurya, K. K., Kumar, A., Kumar, B., Somayajulu, K. & Bhagavannarayana, G. (2011). *J. Appl. Cryst.* **44**, 839–845.
Lal, K. & Bhagavannarayana, G. (1989). *J. Appl. Cryst.* **22**, 209–215.
Lal, K., Bhagavannarayana, G. & Virdi, G. S. (1991). *J. Appl. Phys.* **69**, 8092–8095.
Lerner, P., Legras, E. & Dumas, J. P. (1966). *J. Cryst. Growth*, **3/4**, 231–235.
McMillen, C., Thompson, D., Tritt, T. & Kolis, J. (2011). *Cryst. Growth Des.* **11**, 4386–4391.
Nassau, K., Levinstein, H. & Loiacono, G. (1966). *J. Phys. Chem. Solids*, **27**, 989–996.
Riscob, B., Bhatt, R., Vijayan, N., Bhaumik, I., Ganesamoorthy, S., Wahab, M. A., Rashmi & Bhagavannarayana, G. (2013). *J. Appl. Cryst.* **46**, 601–609.
Schlarb, U. & Betzler, K. (1994). *Phys. Rev. B*, **50**, 751–757.
Senthil Kumar, K., Moorthy Babu, S. & Bhagavannarayana, G. (2011). *J. Appl. Cryst.* **44**, 313–318.
Shen, H. Y., Xu, H., Zeng, Z. D., Lin, W. X., Wu, R. F. & Xu, G. F. (1992). *Appl. Opt.* **31**, 6695–6697.
Sidorov, N. V., Palatnikov, M. N., Gabrielyan, V. T., Chufyrev, P. G. & Kalinnikov, V. T. (2007). *Inorg. Mater.* **43**, 60–67.
Sugh, K., Iwasaki, H., Miyazawa, S. & Nuzeki, N. (1973). *J. Cryst. Growth*, **18**, 159–166.
Sweeney, K. L., Halliburton, L. E., Bryan, D. A., Rice, R. R., Gerson, R. & Tomaschke, H. E. (1985). *J. Appl. Phys.* **57**, 1036–1044.
Tauc, J. C. (1972). *Optical Properties of Solids*, p. 362. Amsterdam: North Holland.
Tsai, P., Sun, M., Chia, C., Lu, H., Lin, S., Hu, M. & Lee, J. (2008). *Appl. Phys. Lett.* **92**, 161902.
Volk, T., Rubinina, N. & Wöhlecke, M. (1994). *J. Opt. Soc. Am. B*, **11**, 1681–1687.
Wallace, C. A. (1970). *J. Appl. Cryst.* **3**, 546–547.
Wempal, S. H. & Didomenico, M. (1969). *J. Appl. Phys.* **40**, 735–752.
Wicks, B. J. & Lewis, M. H. (1968). *Phys. Status Solidi B*, **26**, 571–576.
Yamamoto, J. K., Kitamura, K., Iyi, N., Kimura, S., Furukawa, Y. & Sato, M. (1992). *Appl. Phys. Lett.* **61**, 2156–2158.
Yan, W., Kong, Y., Shi, L., Xie, X., Li, X., Xu, J., Lou, C., Liu, H., Zhang, W. & Zhang, G. (2004). *Phys. Status Solidi A*, **201**, 2013–2020.
Yao, S., Wang, J., Liu, H., Hu, X., Zhang, H., Cheng, X. & Ling, Z. (2008). *J. Alloys Compd.* **455**, 501–505.
Zhang, Q.-R. & Feng, X.-Q. (1991). *Phys. Rev. B*, **43**, 12019–12024.
Zhen, X., Zhao, L. & Xu, Y. (2003). *Appl. Phys. B*, **76**, 655–659.
Zhong, G., Jin, J. & Wu, Z. (1980). *Proceedings of 11th International Quantum Electronic Conference: IEEE*, Cat. No. 80 CH1S61-0, p. 631. Washington, DC: Optical Society of America.
Zhou, W. Z., Cao, F. T., Xu, J., Zhong, W. L. & Wang, H. F. (1990). *Ferroelectrics*, **108**, 183–186.
Zhou, Y., Wang, P. & Tan, H. (1991). *Frontiers of Materials Research: Electronics and Optical Material*, edited by M. Kong & L. Huang, p. 649. Amsterdam: Elsevier.